Serial weighting of micro-objects with resonant microchanneled cantilevers

D Ossola[1], P Dörig[1], J Vörös[1], T Zambelli[1] and M Vassalli[2]

[1] Laboratory of Biosensors and Bioelectronics, Institute for Biomedical Engineering, ETH Zurich, Zurich 8092, Switzerland

[2] Institute of Biophysics (IBF), National Research Council (CNR), Via De Marini 6, Genova I-16149, Italy

E-mail: massimo.vassalli@cnr.it

Abstract. Atomic Force Microscopy (AFM) cantilevers proved to be very effective mass sensors. The attachment of a small mass to a vibrating cantilever produces a resonance frequency shift that can be monitored, providing the ability to measure mass changes down to few molecules resolution. Nevertheless, the lack of a practical method to handle the catch and release process required for dynamic weighting of microobjects, strongly hindered the application of the technology beyond proof of concept measurements. Here a method is proposed in which FluidFM hollow cantilevers are exploited to overcome the standard limitations of AFM-based mass sensors, providing high throughput single object weighting with picogram accuracy. The extension of the dynamic models of AFM cantilevers to hollow cantilevers was discussed and the effectiveness of mass weighting in air was validated on test samples.

Keywords: AFM, mass sensor, FluidFM, cantilever dynamics
Submitted to: *Nanotechnology*

1. Introduction

The exploitation of nanotechnology in the field of biology and medicine led researchers to the adoption of new perspectives to the study of the living matter. In particular, one of the main breakthroughs has been the possibility to move from ensemble measurements down to the study of single objects (cells and even molecules) [1]. This paradigm change allowed to get rid of the intrinsic diversity in biological systems, no longer focusing only on average values, but acquiring the full distribution or following the fate of single cells one at a time [2]. The opportunities offered by this approach are now being exploited in several fields, spanning from basic research to accurate and personalized diagnosis [3].

Nowadays, single cells can be quantitatively measured in terms of their physical properties, and the change in any parameter can be tentatively correlated with the physiological state of the cell itself [4]. Among all measurable parameters, the (bio)mass of cells is known to encode relevant information. The so called dry-mass of cells has been used to measure the quantity and quality of cell populations for long time [5] and the reduction of this parameter to the single cell level is expected to provide a valuable biological indicator. Several approaches have been proposed to estimate cell mass through the measurement of volume [6, 7], leading to fast and effective devices [8]. Nevertheless, only few methods have been proposed to directly measure the weight of micrometric objects, and none of them is able to reach a reasonable throughput and ease of use while tailoring single cells.

The main issue while looking for a method to measure single cell mass, is the needed sensitivity. Biological cells weight in the range of 1-1000 pg, so that a resolution of few pg is required to obtain reliable results and to follow mass changes in real-time (as a reference, living cells are expected to change their mass of about 6% during the whole cell cycle [9]). The most promising approach to gain high resolution measurement of single microscopic objects seems to be the exploitation of resonant micro-mechanical systems [10] and, in particular, atomic force microscopy (AFM) cantilevers [11, 12].

In short, the dynamics of an AFM cantilever is well approximated by a simple harmonic oscillator which shows a resonance frequency f_0 linked to the mass experienced by the cantilever through a trivial relation [12]:

$$f_0 = \frac{1}{2\pi}\sqrt{\frac{\kappa}{m_{eff}}} \tag{1}$$

where κ is the elastic constant and m_{eff} some effective mass [13]. In principle, the addition of a small mass δm to the cantilever will shift the resonance frequency towards lower values, so that an estimate of δm can be obtained by measuring the frequency shift of a calibrated cantilever:

$$\delta m = \frac{\kappa}{(2\pi)^2}\left[\frac{1}{f_1^2} - \frac{1}{f_0^2}\right] \tag{2}$$

where f_1 is the resonance frequency measured after the addition of the mass δm. Measuring the mass of single objects thus becomes a matter of letting them attach to a vibrating cantilever in a condition in which the resonance frequency change can be monitored. This approach proved to be very effective for single sub-micrometric object [14] and fluid droplets [15] weighting, and device miniaturization led to drastic improvements of the sensitivity to mass changes, pushing researchers to race towards the theoretical detection limit [16]. Recently, a single carbon nanotube resonating at 2 GHz enabled to sense adsorbed mass changes with a resolution of 1.7 yg (1 yg = 10^{-24} g), corresponding to the mass of a proton [17]. Unfortunately, the resolution provided by AFM resonating cantilevers comes totally at the expenses of the usability of the system for every day applications. Measuring the mass of a single microscopic object faces the tricky step of attaching the target to the cantilever. The most used approach consists of functionalizing the cantilever surface (i.e. with an antibody) to obtain a specific adhesion of selected objects [14, 18]. In addition, the use of glue was also proposed to catch selected objects on a microscopy slide and to measure their mass [19]. All these approaches have several limitations, among which the more critical are the difficulty to determine the attachment position on the cantilever and the non reversibility of the adhesion procedure. This last point is also the main bottleneck of all the approaches that have been proposed so far, requiring to change the cantilever between two consecutive measurements.

In this work we propose a method to provide single micro-object mass measurement with high accuracy, typical of AFM cantilevers, and improved usability. The method is based on the exploitation of FluidFM cantilevers [20], micro-fabricated hollow cantilevers, with an aperture at the free end, connected to an external microfluidic circuit allowing to apply positive and negative pressures. This system proved to be able to effectively catch and release single micro object by the help of the internal pressure [21] and here we present the exploitation of the device towards precise and fast single micro-object capture and dynamic weighting.

2. Experimental Methods

2.1. Atomic Force Microscopy (AFM)

Tipless FluidFM cantilevers with 2 μm circular aperture were used as received. The cantilevers were received glued on a Cytoclip and were used in combination with a FlexAFM system (Nanosurf, Liestal, Switzerland) and a programmable pressure controller (Cytosurge, Zürich, Switzerland). Where necessary, a Lock-In amplifier (Zürich Instruments, Zürich, Switzerland) was used in Phase-Lock-Loop (PLL) configuration. The cantilever was acoustically excited through a high-frequency piezo positioned in the AFM's probeholder. The excitation signal was generated within the Lock-in amplifier and connected to the piezo excitation input of the FlexAFM controller.

The spring constant was estimated with the Sader method [22], providing values for the selected cantilevers in the order of 2 N/m.

2.2. Trapping and manipulating beads

5 μm, borosilicate glass beads (SPI supplies, West Chester, USA) have been deposited as received on the glass bottom of a WillCo dish (WillCo Wells, Amsterdam, The Netherlands) with the help of a needle. The beads have a reported density of 2.50-2.55 g/cm^3 and a NIST certified mean diameter of 5.1 $\pm$ 0.5 μm. The air trapping protocol was based on the procedure developed in fluid [23, 24], and it consisted in approaching an isolated bead with the FluidFM probe with a setpoint of about 20 nN; when in contact, a sucking pressure of -800 mbar was applied with the pressure controller. Under optical control, the FluidFM aperture was carefully aligned with the bead and, when the bead was trapped (gentle tapping with a finger on the AFM's table can facilitate immobilization), the cantilever was lifted and retracted enough to avoid long-range interaction forces (clearly visible in term of cantilever bending and also affecting dynamic properties). The application of a negative pressure is fundamental to guide the bead exactly to the aperture, but once in place, additional forces contribute to take the bead attached to the cantilever, so that small positive pressures do not induce the detachment. To release the bead, the cantilever was brought in proximity of the substrate (about 10 μm) and maximum overpressure ($>$ 1000 mbar) was applied with the pressure controller or with the help of a syringe. Due to electrostatic force, the bead is attracted onto the glass surface again; proximity to the glass substrate is needed to avoid reattachment of the bead to the cantilever body. In the case that overpressure was not enough to release the trapped bead, or if the bead sticked onto the body of the cantilever, strong vibrational excitation of the cantilever (5 V excitation amplitude, resulting in $>$1000 nm oscillation amplitude) was always successful to clean the cantilever. The AFM was mounted on top of an inverted optical microscope (Axiovert 100 TV, Carl Zeiss AG, Jena, Germany) equipped with a AxioCam CCD camera (Carl Zeiss Microimaging GmbH). Optical snapshots and time course movies were acquired with the open-source micromanager software [25].

2.3. Yeasts

Dried yeasts (*Saccharomyces cerevisiae*) where purchased from a local store. A scalpel was used to carefully smash the aggregates into smaller particles and the resulting powder was collected directly in the WillCo dish. After treatment, single, isolated yeasts were clearly visible and could be aimed and immobilized using the same protocols developed for the beads (see previous section).

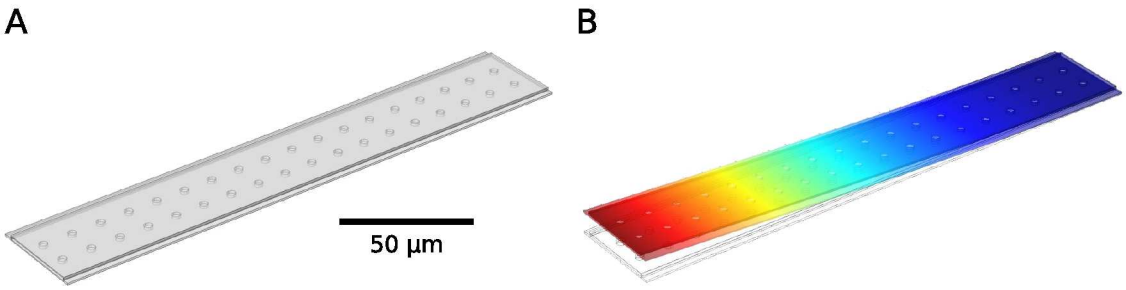

Figure 1. A| Cantilever geometry adopted in the COMSOL simulations; B| Results of simulations for cantilever bending upon force application on the tip. The colors encode the vertical deflection, from blue (no displacement) to dark red (max displacement).

2.4. Finite elements modeling (FEM)

The FluidFM cantilever has geometrical features which cannot be covered by analytical expression, in particular the pillars in the channel and the pyramidal end. To obtain an accurate estimate of the behavior of geometric and dynamic quantities (elastic constant and resonance frequency), the cantilever was modeled using finite elements and the relevant quantities were numerically calculated through COMSOL Multiphysics (COMSOL Inc., Burlington MA, USA) exploiting the Solid Mechanics module. Boundary conditions were chosen by fixing one end of the cantilever (constraining to zero the displacement of the corresponding elements). The cantilever was simulated along its full length of 200 μm with a channel height of 1 μm and a wall thickness of 350 nm. The stabilization pillars were included as cylinders of 3 μm diameter with 11 μm spacing. The cantilever also features winglets of 700 nm height and 3 μm width along the full length (See Fig. 1) that are needed for the production process [26, 23]. The material properties of the cantilever are those of the COMSOL material library for silicon nitride.

2.5. Frequency spectra acquisition

Frequency spectra were acquired in air using an external lock-in amplifier (Zürich Instruments, Zürich). This device was connected to the signal access module of the AFM to synchronize the acquisition of the deflection and the driving sinusoidal signal was sent to the dither piezo near the cantilever. For each measurement, a large 200 kHz frequency sweep was performed, to identify the resonance peak, and a zoom in was thus performed in a range of 20 kHz. The excitation amplitude was set to obtain a maximum oscillation signal of about 800 mV, corresponding to about 90 nm oscillation amplitude. To calculate the resonance frequency, a Lorentzian curve was fitted to the peak of the acquired signal. Repeating the whole measurement procedure led to discrepancies lower than 1 Hz, negligible with respect to all other experimental sources of error. All measurements were carried out far from the substrate, to avoid the effect of long-range

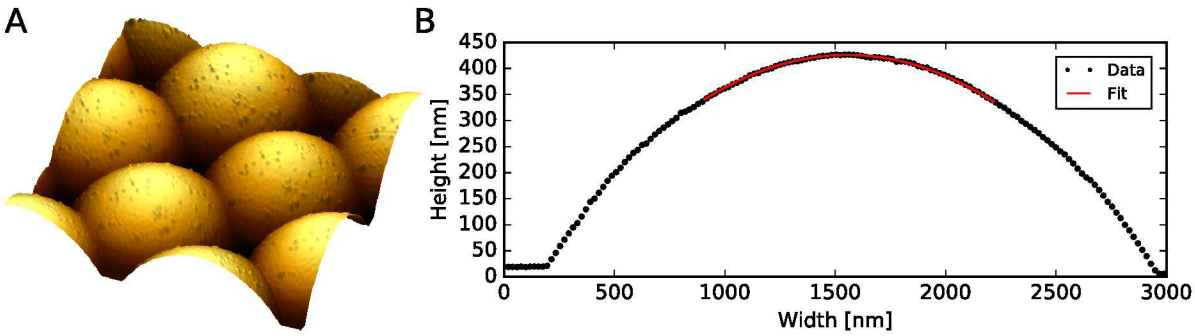

Figure 2. A] Example of convolved image obtained by scanning a catched bead on the TGT1 calibration grating. Figure is 5μm x 5μm wide; total vertical range is about 500nm. B] Profile extraction and second order fit needed to calculate the sphere radius.

forces (usually at maximum distance allowed by the motorized foot of the AFM)

2.6. AFM imaging of the trapped beads

For calibration purposes, the mass of 5 μm NIST standard glass beads (SPI supplies, West Chester, USA) was determined starting from provider data sheet. The density of the material is declared in the range between 2.50 g/cm^3 and 2.55 g/cm^3, providing a 1% maximum relative error in the mass estimate when taking ρ=2.525 g/cm^3. The provider certified diameter lies in the range of 5.1 $\pm$ 0.5 μm, thus providing a large error to the mass estimate of about 30%. To eliminate this contribution, the radius of the caught beads was measured by means of the AFM. After immobilization of the bead at the aperture of the FluidFM tipless probe, an AFM image was acquired on a TGT1 calibration grating (MDT Co, Zelonograd, Russia), featuring an array of sharp probes with 10 nm nominal radius. The resulting image is a convolution of the sphere with the delta-like substrate (see Fig. 2A). To measure the bead radius, a profile was extracted around the top of the sphere (catching the circumference of maximal radius) and a second order polynomial curve was fitted on it (see Fig. 2B). The diameter of the sphere is thus calculated as the inverse of the coefficient of the second order term in the fit. All calculations were done using the free software Gwyddion [27] and the full procedure was repeated over different images, profiles and positions, obtaining an intrinsic uncertainty under 1%.

3. Results and discussion

3.1. Frequency measurement

The shift in the resonant frequency due to the adhesion of an object to the cantilever was measured as described in the corresponding Methods section. Fig. 3A shows an example of a typical experimental result while catching reference beads (see Methods). To evaluate the stability of the measurement, the unloaded spectrum was always recorded

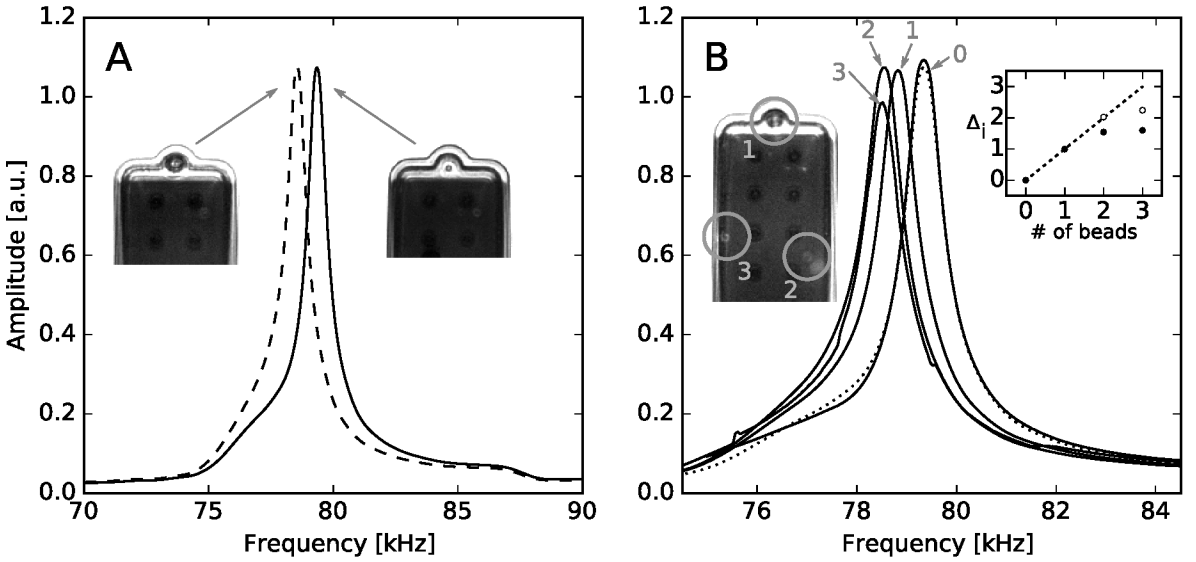

Figure 3. A] Frequency response of the FluidFM prior (solid line) and after (dashed line) catching a bead; inset images show a close-up view of the tip of the cantilever in the two conditions. B] Oscillation spectra acquired on the bare cantilever (0) and after serial catching of bead 1 (1), bead 2 (2) and bead 3 (3); the dashed line corresponds to the spectrum obtained at the end of the experiment, after downloading all beads. The inset picture on the left highlights the position of the three beads. The inset graph shows the relative inverse frequency shift (black circles, see text for details) as a function of the number of caught beads, showing that the behavior deviates from the expected trend (dashed line) for beads attached far from the tip. White circles correspond to the value corrected for the position of the bead along the cantilever.

twice, before loading the bead and after unloading it. No statistically relevant difference was appreciated in any situation, even after long activity of the cantilever (see for example the two spectra labeled 0 in fig 3B which are separated by about 1 hour of repeated catch-release activity of multiple beads).

A crucial aspect in the use of AFM cantilevers as mass sensors and, in particular, a prerequisite for the application of the Equation 2, is the ability to catch the bead exactly at the tip of the cantilever [28]. The effect of the position of the micro-object on the cantilever dynamics, and thus on the measured mass, was extensively studied [29] and an experimental insight of this phenomenon can be observed in Fig. 3B. During the experiment, a first bead was captured with the FluidFM cantilever, by the application of a negative pressure at its apex (see Methods). In this configuration the position of the bead can be considered at the tip. A corresponding frequency change was measured, from f_0 to $f_1 < f_0$, obtaining an inverse quadratic frequency shift Δ_1 of:

$$\Delta_1 = \frac{1}{f_1^2} - \frac{1}{f_0^2} = 2.106 \cdot 10^{-12} Hz^{-2} \tag{3}$$

Accordingly with Equation 2, adding a second and third bead of about the same mass would likely produce a frequency shift so that $\Delta_2 = 2\Delta_1$ and $\Delta_3 = 3\Delta_1$. This assumption was verified experimentally verified. As reported in the Methods section, when delivering

a captured bead, it is suggested to be nearby the sample, so that beads can stick to the surface after detachment. If the unloading procedure is performed far from the sample, it can happen that the bead, after detachment, re-attaches to the cantilever in a random position. This issue was exploited to deliberately induce the attachment of additional beads to the body of the cantilever. During the experiment, other 2 beads were caught in different positions (see the inset picture of figure 3), and the corresponding spectrum was measured at each addition. The inset graph of figure 3 reports the corresponding behavior of Δ_i/Δ_1 (black filled circles). As mentioned, having the masses almost the same weight, it is expected that the resulting ratios Δ_i/Δ_1 would stick on a straight line with slope 1 (dashed line in the inset). As clearly visible, the frequency change associated to masses 2 and 3 (that are far from the tip) is not following the expected curve.

The effect of the position is associated to the shape of the corresponding mode and, in principle, it can be taken into account [30]. If x is the coordinate along the major axis of the cantilever, and a mass δm, smaller with respect to the cantilever mass m_0, is put at a position x_M (counted from the fixed end of the cantilever of total length L), the expected resonance frequency of the first mode follows (see [30]):

$$\omega_M^2 = \omega_0^2 \left(1 + \frac{\delta m}{m_0} U_0(x_M)\right)^{-1} \tag{4}$$

where ω_0^2 is the unloaded resonance frequency and $U_0(x_M)$ is the shape of the first mode for a clamped beam [31] calculated in the position x_M. From this equation, it is possible to calculate the resonance frequency ω_T that the same mass would induce if attached exactly to the tip, by the following relation:

$$\frac{1}{\omega_T^2} = (1+\alpha)\frac{1}{\omega_M^2} - \alpha\frac{1}{\omega_0^2} \tag{5}$$

where α is a geometric coefficient ranging between 0 and 1, associated to the mode shape calculated in x_M and at the tip end x_T:

$$\alpha = \frac{U^2(x_T)}{U^2(x_M)} - 1 \tag{6}$$

The position of the three beads in figure 3B was visually measured and Equation 6 was applied to correct the frequency, obtaining the empty circles in Fig. 3B. After correction, the point corresponding to the addition of the second mass perfectly follows the linear behavior, while the third point still does not. In fact, the correction factor of Eq. 6 is exact only for particles attached along the main axis of the cantilever, but it still holds for small distances, for which the shape of the mode itself is not significantly altered by the addition of the particle [29]. As a matter of fact, a configurations in which the sphere is attached near the edge of the cantilever, such as for particle 3, is strongly altering the cantilever dynamics, and the frequency change cannot be simply recovered, so that this situation must be avoided while using the system as a mass sensor.

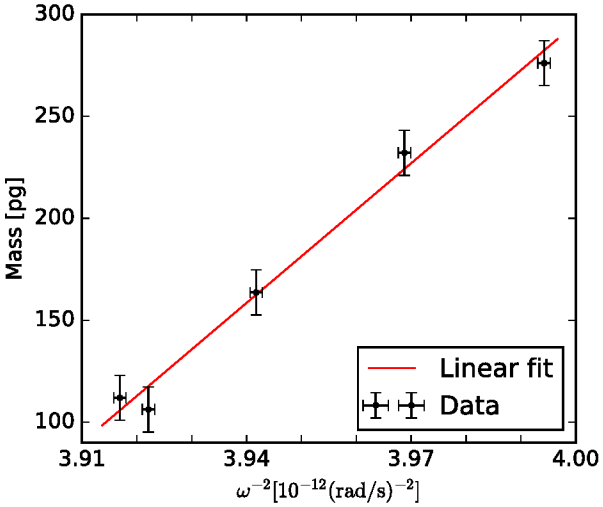

Figure 4. Mass of reference sphere attached to the cantilever plotted as a function of the corresponding inverse square of the resonance frequency. The slope of the linear fit provides the calibrated elastic constant of the cantilever.

3.2. Cantilever calibration

FluidFM technology features a nano-pipette with an integrated deflection sensor system (the standard AFM optical beam deflection method, OBDM). In order to convert the relative OBDM signal to a quantitative measure of the force, it is necessary to calibrate the static elastic constant κ of the cantilever. This issue has been widely addressed for standard AFM cantilevers [32, 33], and nowadays the most adopted approach relies on the theoretical work of Sader [22]. The advantage of this method, with respect to the thermal calibration [34], is that it does not require to engage the tip to the sample, preserving the cantilever integrity (that can be relevant for special FluidFM cantilevers), and being applicable even when rigid regions on the sample are not trivial to find (e.g. working with confluent living cells). The standard Sader method [22], initially conceived for rectangular cantilevers, related the elastic constant to the first mode resonance frequency:

$$\kappa = 0.1906 \rho_f W^2 L Q_f \Gamma(\omega) \omega^2 \tag{7}$$

where ρ_f is the density of the medium, $\Gamma(\omega)$ the hydrodynamic function of the surrounding fluid, L and W the length and width of the cantilever, respectively. Interestingly, the Sader formula does not depend on the thickness of the cantilever and all the assumptions of the original paper are still valid for hollow cantilevers, as long as the section can be considered constant along the length of the cantilever. This hypothesis is generically verified by FluidFM cantilevers, apart for the presence of pillars inside the hole [21]. To evaluate the role of the pillars (and thus the applicability of the Sader formula) a FEM simulation was carried out for a hollow cantilever with and without pillars (see figure 1). To obtain the static elastic constant, a defined force was applied to the free end of the cantilever (represented in terms of FEM meshes, see figure 1A) and the correspond-

ing deformation pattern was recorded for different forces (see figure 1B). As expected, the obtained κ was identical to the one estimated using the Sader method on a filled cantilever of the same external geometry and the pillars had a very small impact on the spring constant, about 1%.

The original Sader method was demonstrated for rectangular cantilevers, but it was next generalized [35] to obtain an expression for arbitrary shape plan-view cantilevers similar to Eq.7 in which the effect of the geometry is incorporated in a coefficient of hydrodynamic origin, to be calculated (theoretically or numerically) for each cantilever shape. As a consequence of this general formula, it was recently argued that for each batch of cantilevers (i.e. with the same shape but small differences eventually due to fabrication tolerances), it is sufficient to calibrate one cantilever, namely obtaining κ_R, to obtain the calibration for all other cantilevers by simply measuring their resonance frequency f and quality factor Q [36]. In particular, if f_R and Q_R are the frequency and quality factor for the reference cantilever, respectively, the calibration of a generic cantilever of the batch can be calculated as:

$$\kappa = \kappa_R \frac{Q}{Q_R} \left(\frac{f}{f_R} \right)^{2-\alpha} \tag{8}$$

where $\alpha = 0.7$ is a constant coefficient [35]. In order to obtain the reference calibration, the Cleveland method was used [31]. This approach only relies on the Equation 2 and the use of a set of calibrated spheres. This approach provides a direct measure of the elastic constant with a low uncertainty, claimed to be under 10%, and the approach is valid for any cantilever shape, provided that the masses are added exactly at the tip position. In addition, this method does not rely on dynamic coefficients, to be calculated or measured for each cantilever. Nevertheless, the method has been poorly exploited in literature, due to the tricky and painful procedure of adding calibrated masses at the end of a micrometric cantilever. This limit is overcome by the use of FluidFM with the proposed catch-and-release procedure, but obtaining a good estimate still requires to image a set of calibrated spheres over a reference grating (see Methods) that is a time consuming procedure. For optimal calibration of FluidFM cantilevers we thus propose to use the Cleveland method for one cantilever in each batch, and propagate the calibration to all other cantilevers of the same batch through the use of Equation 8. Figure 4 shows the experimental results of the Cleveland method for a selected cantilever of the batch, providing a calibration constant $\kappa = 2.03 N/m$ with a measurement error under 10%.

3.3. Role of the pressure

The resonance frequency of the FluidFM cantilever is expected to be influenced by an internal applied pressure. This effect was experimentally evaluated by measuring frequency changes as a function of the internal pressure P for both open-end and closed-end configurations (see Fig. 5). The application of a pressure to the internal channel by means of the FluidFM pump induces a difference between internal and external pressure

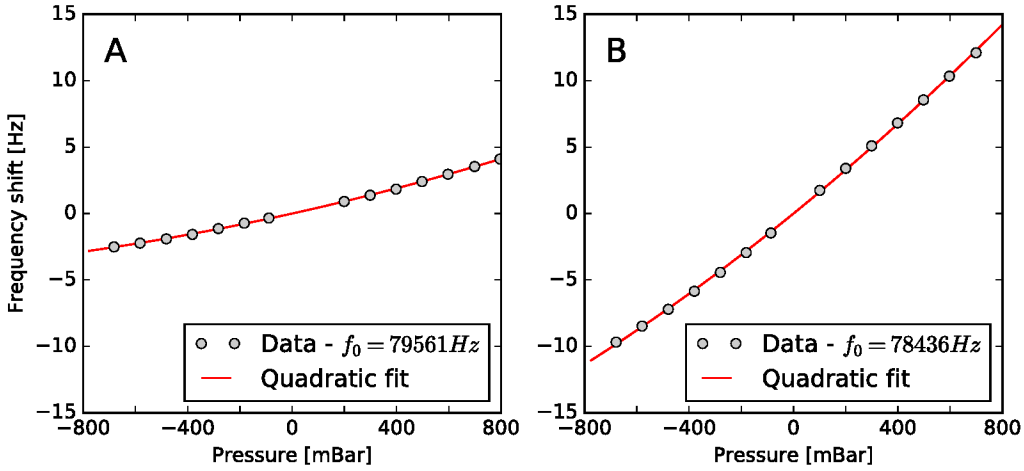

Figure 5. Shift of resonance frequency as a function of the pressure applied in the inner channel of the holed cantilever. Results are reported for the open-end (A) and closed-end (B) configurations. Unloaded resonance frequency f_0 for no pressure is reported in the figure legend.

that, in turn, produces a mechanical stress to the vibrating structure. The geometry of the cantilever thus becomes slightly modified, potentially inducing a change in the area moment of inertia that is directly related to the elastic constant. Figure 5 depicts the results obtained while measuring the resonance frequency of a FluidFM cantilever as a function of the internal pressure, in a range of ±800 mBar (not enough to detach any bead, see Methods). Measurements were repeated for the free cantilever (Fig. 5A) and after having caught a glass bead (closed end, Fig. 5B). The results show that the frequency shift associated to the presence of a pressure can be reasonably neglected if an error of about 1% can be sustained or, otherwise, measurement of the resonance frequency for $P = 0$ should be preferred.

The precise behavior of ω as a function of P presented in Fig. 5 cannot be simply recovered analytically, but a rule-of-thumb estimation can be obtained describing the FluidFM cantilever as a thin hollow cylinder of external diameter D and thickness T. For this simplified geometry, an analytical expression exists that links the change in diameter, δD of the cylinder to the internal pressure P [37]:

$$\delta D = \frac{D^2}{4TE}(2-\nu)P \tag{9}$$

where E and ν are the Young modulus and Poisson ratio, respectively. The area moment of inertia I_A of a hollow cantilever can be calculated as:

$$I_A = \frac{WT^3}{12} - \frac{W_c T_c^3}{12} \tag{10}$$

where W and T are the external dimensions (width and thickness) while W_c and T_c are the internal dimensions of the channel. If the lateral dimensions change proportional to P, according to Equation 9, I_A will behave as P^4. Moreover, the resonance frequency is strictly related to I_A [12] and it goes as the square root of I_A, so that a quadratic

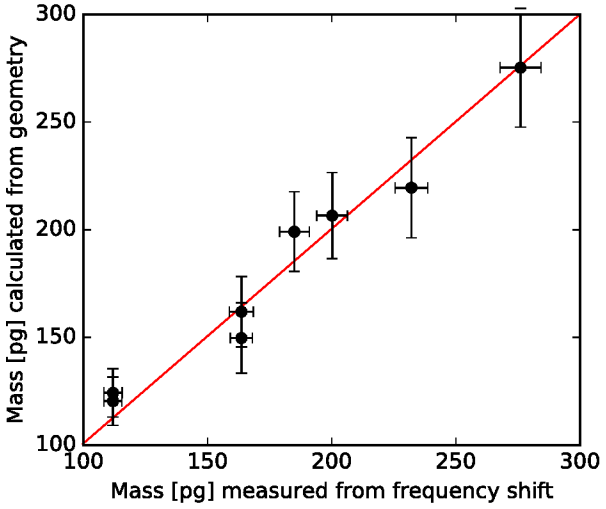

Figure 6. Comparison of the mass of reference spheres obtained by the frequency shift method with the expected mass calculated from the geometry of the spheres. The continuous line corresponds to the expected behavior.

behavior $\omega \propto P^2$ is expected to occur. In fact, the solid lines in figure 5A and 5B represent a quadratic trend, perfectly fitting to the data. Nevertheless, the coefficients of the fit cannot be simply related to the geometry of the cantilever, because several boundary effects should be taken into account. The open configuration can no longer be considered at constant pressure, and the dynamics of the system in this configuration can lead to instabilities and even chaotic behavior [38]. Nevertheless, for the range of pressures that can be applied with the FluidFM system, the dynamics seems to remain in the linear regime and the quadratic behavior still holds, but experiencing an effective pressure lower than the value measured at the entrance of the channel.

3.4. Measuring masses from frequency shift

Once the elastic constant of the cantilever has been calibrated, as suggested in Section 3.2, Equation 2 can be used to estimate the mass of a micrometric object with a measurement error of about 10%, mainly associated to the incertitude in the value of κ. To verify the method, a set of frequency-based weightings was performed on a sample of reference beads, comparing the results with the expected mass, as calculated from the geometry (see Section 3.2 and corresponding Methods). The results of the experimental verification are presented in Fig. 6, showing a good match of the two approaches.

The effectiveness of the overall weighting procedure was thus validated on a biological sample: a population of yeast cells. Besides being biologically relevant, measuring the mass of single yeasts in a population can also have biotechnology relevance, for example to identify the state of the population in relation to the production of recombinant proteins [39], and it has been addressed for more than half a century [40]. Single yeast (*Saccharomyces cerevisiae*) cells are few μm large and they typically weight 10-

100pg [41], perfectly fitting the measurement capabilities of the proposed FluidFM-based approach. Figure 7 shows the salient events of a weighting procedure on a single yeast cell. A resonance spectrum of the cantilever was acquired at the beginning of the experiment, recording f_0 and, after having identified a potential target, the cantilever was put in contact with the substrate in a clean area, by means of the standard AFM auto-approach procedure. After reaching the contact, the cantilever was retracted to the maximum distance allowed by the vertical piezo of the AFM (to avoid touching cells or debris during the motion) and it was moved above the aimed cell using the AFM software commands. The cantilever was thus brought into contact over the yeast cell and a negative pressure was applied. Sometimes, to facilitate the detachment of the cells from the glass slide, a small vibration of the sample was induced in this configuration by gently tapping on the microscope stage. To verify the attachment of the cell, the cantilever was moved while still near contact. For each caught cell, the resonance spectrum was thus acquired in a position far from the substrate and the loaded frequency f_1 measured. Finally, the particle was downloaded by imposing a huge vibration of the cantilever with the internal dither piezo (the one normally used for non-contact AFM imaging) and the unloaded frequency f_0 was measured again, to verify the effective delivery of the biological material. This measurement procedure was repeated, collecting and weighting cells with a throughput of about 10 cells/hour, mainly limited by the difficulty in finding isolated cells in the sample under examination. Figure 7F shows the spectra acquired for the cell aimed in frame B of the same figure, providing a shift of 52Hz, from $f_0 = 78.146$kHz to $f_1 = 78.094$kHz, corresponding to a mass of about 11pg..

4. Conclusions

FluidFM technology is an emerging approach for force-controlled micro-object manipulation and analysis. Here a method was presented to extend the technique to weight single cells with an unprecedented mix of sensitivity and usability. AFM cantilevers were already used as high resolution mass sensors [11], but one of the main limiting factors in the precise determination of the added mass has been the need to know the exact attachment position [12]. This issue is intrinsically solved by using FluidFM cantilevers, for which the aimed particles are directly caught at the aperture near the tip or, even in case of specialized geometries, in a well defined position that can be taken into account for the determination of the loaded resonance frequency (see Section 3.1). Additionally, attaching micro-objects to the AFM cantilever for sensing purposes constitutes a tricky, time-consuming and fault-prone procedure, so that the suggested approach [19, 14] never converted in a widespread method.

The adoption of FluidFM for mass sensing provides a definite breakthrough, allowing to collect a statistically relevant set of single object measurements in a reasonable time. As a matter of reference, the proposed immobilization procedure requires only a couple of minutes per particle, including the force controlled approach, suction, withdraw of

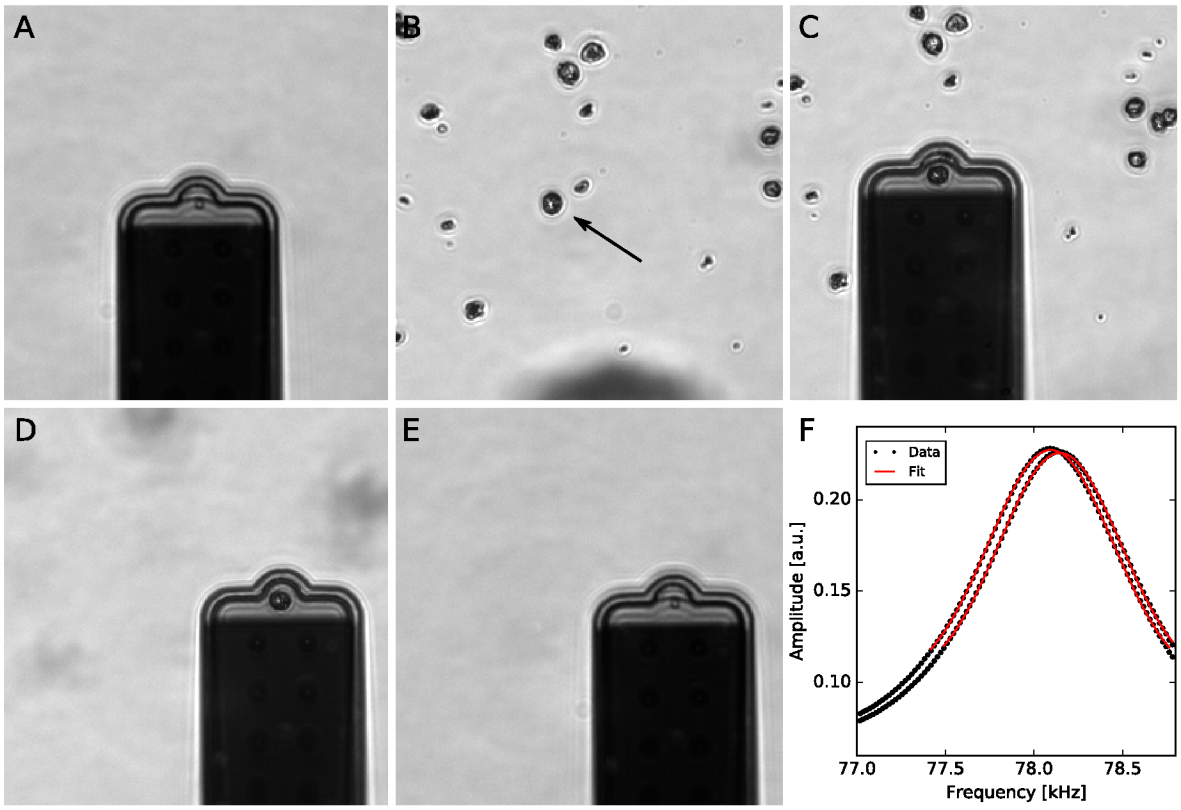

Figure 7. Sequence of optical images captured during a weighting procedure of a single yeast cell. The cantilever is kept far from the substrate to acquire the free spectrum (image A) and a specific target on the substrate is selected (arrow in frame B). The cantilever is thus brought into contact on top of the target and a negative pressure is applied (C). When moving the hollow cantilever far from the substrate, the target remains attached to the tip (frame D) and the loaded spectrum can be acquired. Finally, by imposing a strong positive pressure ($>$ 800mBar) or by shaking the cantilever with the dither piezo of the AFM (see Methods), the target is released and the weighting procedure can be repeated. Frame F shows the spectra before (right curve, corresponding to frame A) and after (left curve, frame D) catching a yeast cell. Images are about 75 μm x 75 μm.

the probe from the substrate, frequency spectrum acquisition and micro object release. Collecting a statistically relevant set of single cell mass measurements would allow to address open biological questions, by recording the whole distribution of events, instead of looking at the average value only. In particular the ability to finely measure the growth rate of single cells could allow to infer about unclear mechanism underlying cell growth regulation [42]. To extend the approach of FluidFM mass weighting even more towards biological applications, the next challenge will be to assess the measurement procedure to work in liquid environment. To such an extent, the frequency detection procedure will need to be modified, to get rid of the reduced quality factor in liquid environment, through the exploitation of Q-enhancement [43, 44] or self excitation approaches [45, 46].

5. Acknowledgements

The authors acknowledge the Swiss National Science Foundation for supporting the activity through the International Short Visits grant number IZK0Z2_155218 (to M.V.) and the Interdisciplinary Project CR23I2_135535 (to T.Z.).

References

[1] Andersson H and van den Berg A 2004 *Current Opinion in Biotechnology* **15** 44–49 ISSN 0958-1669 URL http://dx.doi.org/10.1016/j.copbio.2004.01.004

[2] Spiller D G, Wood C D, Rand D A and White M R H 2010 *Nature* **465** 736–745 ISSN 1476-4687 URL http://dx.doi.org/10.1038/nature09232

[3] Beckman R A, Schemmann G S and Yeang C H 2012 *Proceedings of the National Academy of Sciences* **109** 14586–14591 ISSN 1091-6490 URL http://dx.doi.org/10.1073/pnas.1203559109

[4] Mescola A, Vella S, Scotto M, Gavazzo P, Canale C, Diaspro A, Pagano A and Vassalli M 2012 *Journal of Molecular Recognition* **25** 270–277 ISSN 0952-3499 URL http://dx.doi.org/10.1002/jmr.2173

[5] Frame K K and Hu W S 1990 *Biotechnology and Bioengineering* **36** 191–197 ISSN 1097-0290 URL http://dx.doi.org/10.1002/bit.260360211

[6] Reshes G, Vanounou S, Fishov I and Feingold M 2008 *Biophysical Journal* **94** 251–264 ISSN 0006-3495 URL http://dx.doi.org/10.1529/biophysj.107.104398

[7] Phillips K G, Jacques S L and McCarty O J T 2012 *Physical Review Letters* **109** ISSN 1079-7114 URL http://dx.doi.org/10.1103/PhysRevLett.109.118105

[8] Ferraro P, Wax A and Zalevsky Z (eds) 2011 *Coherent Light Microscopy* (*Springer Series in Surface Sciences* vol 46) (Springer Berlin Heidelberg)

[9] Tzur A, Kafri R, LeBleu V S, Lahav G and Kirschner M W 2009 *Science* **325** 167–171 ISSN 1095-9203 URL http://dx.doi.org/10.1126/science.1174294

[10] Park K, Millet L J, Kim N, Li H, Jin X, Popescu G, Aluru N R, Hsia K J and Bashir R 2010 *Proceedings of the National Academy of Sciences* **107** 20691–20696 ISSN 1091-6490 URL http://dx.doi.org/10.1073/pnas.1011365107

[11] Waggoner P S and Craighead H G 2007 *Lab Chip* **7** 1238 ISSN 1473-0189 URL http://dx.doi.org/10.1039/B707401H

[12] Boisen A, Dohn S, Keller S S, Schmid S and Tenje M 2011 *Reports on Progress in Physics* **74** 036101 ISSN 1361-6633 URL http://dx.doi.org/10.1088/0034-4885/74/3/036101

[13] Cleveland J P, Manne S, Bocek D and Hansma P K 1993 *Review of Scientific Instruments* **64** 403 ISSN 0034-6748 URL http://dx.doi.org/10.1063/1.1144209

[14] Ilic B, Czaplewski D, Zalalutdinov M, Craighead H G, Neuzil P, Campagnolo C and Batt C 2001 *Journal of Vacuum Science & Technology B: Microelectronics and Nanometer Structures* **19** 2825 ISSN 0734-211X URL http://dx.doi.org/10.1116/1.1421572

[15] Arcamone J, Dujardin E, Rius G, Pérez-Murano F and Ondarçuhu T 2007 *J. Phys. Chem. B* **111** 13020–13027 ISSN 1520-5207 URL http://dx.doi.org/10.1021/jp075714b

[16] Ekinci K L 2004 *Journal of Applied Physics* **95** 2682 ISSN 0021-8979 URL http://dx.doi.org/10.1063/1.1642738

[17] Chaste J, Eichler A, Moser J, Ceballos G, Rurali R and Bachtold A 2012 *Nature Nanotechnology* **7** 301–304 ISSN 1748-3395 URL http://dx.doi.org/10.1038/nnano.2012.42

[18] Canale C, Petrelli A, Salerno M, Diaspro A and Dante S 2013 *Biosensors and Bioelectronics* **48** 172–179 ISSN 0956-5663 URL http://dx.doi.org/10.1016/j.bios.2013.04.015

[19] Hassenkam T, Johnsson A, Bechgaard K and Stipp S L S 2011 *Proceedings of the National Academy of Sciences* **108** 8571–8576 ISSN 1091-6490 URL http://dx.doi.org/10.1073/pnas.1009447108

[20] Meister A, Gabi M, Behr P, Studer P, Vörös J, Niedermann P, Bitterli J, Polesel-Maris J, Liley M, Heinzelmann H and et al 2009 *Nano Lett.* **9** 2501–2507 ISSN 1530-6992 URL http://dx.doi.org/10.1021/nl901384x

[21] Dörig P, Ossola D, Truong A, Graf M, Stauffer F, Vörös J and Zambelli T 2013 *Biophysical Journal* **105** 463–472 ISSN 0006-3495 URL http://dx.doi.org/10.1016/j.bpj.2013.06.002

[22] Sader J E, Chon J W M and Mulvaney P 1999 *Review of Scientific Instruments* **70** 3967 ISSN 0034-6748 URL http://dx.doi.org/10.1063/1.1150021

[23] Dörig P, Stiefel P, Behr P, Sarajlic E, Bijl D, Gabi M, Vörös J, Vorholt J A and Zambelli T 2010 *Applied Physics Letters* **97** 023701 ISSN 0003-6951 URL http://dx.doi.org/10.1063/1.3462979

[24] Ossola D, Behr P, Amarouch M Y, Abriel H, Vörös J and Zambelli T 2013 *Biophysical Journal* **104** 502a ISSN 0006-3495 URL http://dx.doi.org/10.1016/j.bpj.2012.11.2771

[25] Edelstein A, Amodaj N, Hoover K, Vale R and Stuurman N 2010 *Current Protocols in Molecular Biology* URL http://dx.doi.org/10.1002/0471142727.mb1420s92

[26] Deladi S, Tas N R, Berenschot J W, Krijnen G J M, de Boer M J, de Boer J H, Peter M and Elwenspoek M C 2004 *Applied Physics Letters* **85** 5361 ISSN 0003-6951 URL http://dx.doi.org/10.1063/1.1823040

[27] Nečas D and Klapetek P 2012 *Open Physics* **10** ISSN 2391-5471 URL http://dx.doi.org/10.2478/s11534-011-0096-2

[28] Golovko D S, Haschke T, Wiechert W and Bonaccurso E 2007 *Review of Scientific Instruments* **78** 043705 ISSN 0034-6748 URL http://dx.doi.org/10.1063/1.2720727

[29] Xie H, Vitard J, Haliyo S and Régnier S 2008 *Journal of Micro-Nano Mechatronics* **4** 17–25 ISSN 1865-3936 URL http://dx.doi.org/10.1007/s12213-008-0005-y

[30] Dohn S, Svendsen W, Boisen A and Hansen O 2007 *Review of Scientific Instruments* **78** 103303 ISSN 0034-6748 URL http://dx.doi.org/10.1063/1.2804074

[31] Cleland A N 2003 *Advanced Texts in Physics* ISSN 1439-2674 URL http://dx.doi.org/10.1007/978-3-662-05287-7

[32] Burnham N A, Chen X, Hodges C S, Matei G A, Thoreson E J, Roberts C J, Davies M C and Tendler S J B 2002 *Nanotechnology* **14** 1–6 ISSN 0957-4484 URL http://dx.doi.org/10.1088/0957-4484/14/1/301

[33] Mendels D A, Lowe M, Cuenat A, Cain M G, Vallejo E, Ellis D and Mendels F 2006 *Journal of Micromechanics and Microengineering* **16** 1720–1733 ISSN 1361-6439 URL http://dx.doi.org/10.1088/0960-1317/16/8/037

[34] Hutter J L and Bechhoefer J 1993 *Review of Scientific Instruments* **64** 1868 ISSN 0034-6748 URL http://dx.doi.org/10.1063/1.1143970

[35] Sader J E, Sanelli J A, Adamson B D, Monty J P, Wei X, Crawford S A, Friend J R, Marusic I, Mulvaney P and Bieske E J 2012 *Review of Scientific Instruments* **83** 103705 ISSN 0034-6748 URL http://dx.doi.org/10.1063/1.4757398

[36] Sader J E and Friend J R 2014 *Review of Scientific Instruments* **85** 116101 ISSN 1089-7623 URL http://dx.doi.org/10.1063/1.4901227

[37] Hearn E J 1997 *Mechanics of Materials 1* iii URL http://dx.doi.org/10.1016/B978-0-7506-3265-2.50023-2

[38] Hu K, Wang Y, Dai H, Wang L and Qian Q 2016 *International Journal of Engineering Science* **105** 93–107 ISSN 0020-7225 URL http://dx.doi.org/10.1016/j.ijengsci.2016.04.014

[39] Palmer S M and Kunji E R S 2012 *Recombinant Protein Production in Yeast* 157–163 ISSN 1940-6029

[40] HADDAD S A and LINDEGREN C C 1953 *Appl Microbiol* **1** 153–156

[41] Mitchison J 1958 *Experimental Cell Research* **15** 214–221 ISSN 0014-4827 URL http://dx.doi.org/10.1016/0014-4827(58)90077-6

[42] Weitzman J B 2003 *J Biol* **2** 3 ISSN 1475-4924 URL http://dx.doi.org/10.1186/1475-4924-2-3

[43] Humphris A D L, Tamayo J and Miles M J 2000 *Langmuir* **16** 7891–7894 ISSN 1520-5827 URL http://dx.doi.org/10.1021/la000766c

[44] Tamayo J, Alvarez M and Lechuga L M 2003 *Sensors and Actuators B: Chemical* **89** 33–39 ISSN 0925-4005 URL http://dx.doi.org/10.1016/S0925-4005(02)00424-0

[45] Paoletti P, Basso M, Pini V, Tiribilli B and Vassalli M 2011 *Journal of Applied Physics* **110** 114315 ISSN 0021-8979 URL http://dx.doi.org/10.1063/1.3665396

[46] Basso M, Paoletti P, Tiribilli B and Vassalli M 2008 *Nanotechnology* **19** 475501 ISSN 1361-6528 URL http://dx.doi.org/10.1088/0957-4484/19/47/475501